CHAPTER 3

EXPERIMENTAL TECHNIQUES

This chapter describes the materials and methods used for the synthesis of polypyrrole nanotubes, polyaniline nanotubes, reduced graphene oxide and their nanocomposites. The basic principles of different experimental techniques used in the present thesis work along with their brief instrumentation have been discussed. Electrochemical characterization techniques employed for investigating the specific capacitance, energy density, power density and cyclic stability have also been presented.

3.1 Materials

Pyrrole (98%, monomer) for the synthesis of polypyrrole nanotubes (PPyNTs) was procured from Sigma-Aldrich. Methyl orange (MO) and ferric chloride ($FeCl_3$) were obtained from Sisco Research Laboratory (SRL). For the synthesis of graphene oxide, graphite powder was purchased from Loba Chemie, sulphuric acid (98%) from Rankem, potassium permanganate and hydrogen peroxide (30%) from Merck. Aniline (99.5%, monomer) for the synthesis of polyaniline nanotubes (PAniNTs) was obtained from Merck. Oxidant ammonium peroxydisulfate and hydrochloric acid (36%) were procured from Merck and Rankem, respectively. For the reduction of graphene oxide (GO), GO-PPyNTs and GO-PAniNTs nanocomposites, hydrazine monohydrate (80%) procured from SD fine chemicals limited (SDFCL) was used as reducing agent. The solvents ethanol, methanol and acetone used for washing the synthesized nanostructures were obtained from Merck. Pyrrole and aniline were distilled under reduced pressure and stored in dark prior to use. All other chemicals and solvents were of analytical grade and were used as-received without further purification. For the preparation of electrodes for electrochemical measurements, indium tin oxide (ITO) coated glass slides were purchased from Macwin India Pvt. Ltd. The physical properties of the materials used for the synthesis of reduced graphene oxide based PPyNTs and PAniNTs nanocomposites in the present work are tabulated in Table 3.1.

Table 3.1: *Some physical properties of the materials used in synthesis*

Physical properties of monomer

Monomer	Molecular formula	Molecular weight (gm/mol)	Melting point (°C)	Boiling point (°C)	Density at 25°C (gm/ml)	Oxidation potential (Volt)
Pyrrole	C_4H_5N	67.09	-23	129	0.967	0.8
Aniline	$C_6H_5NH_2$	93.13	-6.3	184.1	1.02	0.9

Physical properties of oxidant

Oxidant	Molecular formula	Molecular weight (gm/mol)	Melting point (°C)	Boiling point (°C)	Density at 25°C (gm/ml)
Ferric chloride	$FeCl_3$	162.2	306	315	2.898
Ammonium peroxydisulfate	$(NH_4)_2S_2O_8$	228.18	120	-	1.98

Physical properties of solvents and acids

Solvent	Molecular formula	Molecular weight (gm/mol)	Melting point (°C)	Boiling point (°C)	Density (gm/ml)
Acetone	C_3H_6O	58.08	-95	56	0.791
Methanol	CH_4O	32.04	-97.6	64.7	0.791
Ethanol	C_2H_6O	46.06	-114	78.37	0.789
Sulphuric acid	H_2SO_4	98.08	10	337	1.84
Hydrochloric acid	HCl	36.46	-30	61	1.18

Physical properties of chemicals used in synthesis process

Solvent	Molecular formula	Molecular Weight (gm/mol)	Melting point (°C)	Boiling point (°C)	Density (gm/ml)
Graphite	C	12.01	3652-3697	-	2.09-2.23
Methyl orange	$C_{14}H_{14}N_3NaO_3S$	327.34	300	-	1.28
Potassium permanganate	$KMnO_4$	158.03	240	-	2.70
Hydrogen peroxide	H_2O_2	34.01	-0.43	150.2	1.11
Hydrazine hydrate	$NH_2NH_2.H_2O$	50.06	-51.7	120.1	1.02

3.2 Synthesis of polypyrrole nanotubes, reduced graphene oxide and nanocomposites

3.2.1 Synthesis of polypyrrole nanotubes

A reactive self-degrade template method of methyl orange-ferric chloride (MO-$FeCl_3$) as reported by Dai et al. [255] was followed to synthesize PPyNTs. The synthesis procedure was as follows: 0.243 gm (1.5 m mol) of $FeCl_3$ was dissolved in 30 mL of 5 mM (0.15 m mol) MO solution in deionized (DI) water. A flocculant precipitate appeared immediately, which indicates the formation of MO-$FeCl_3$ complex. Subsequently, 105 µL (1.5 m mol) pyrrole was added to the reaction solution. After sometime, the solution appeared black indicating the polymerization of pyrrole. The mixture was allowed to stir at room temperature for 24 h to complete the polymerization. The polymerization reaction occurs on the surface of MO-$FeCl_3$ complex, which acts as a template and directs the growth of PPyNTs. The complex degrades automatically during polymerization due to the reduction of oxidising cations and can be removed during the washing process. The obtained PPy precipitate was washed with DI water and methanol several times until the filtrate became colorless followed by drying at 50 °C for 24 h. The block diagram for the synthesis process is shown in Figure 3.1.

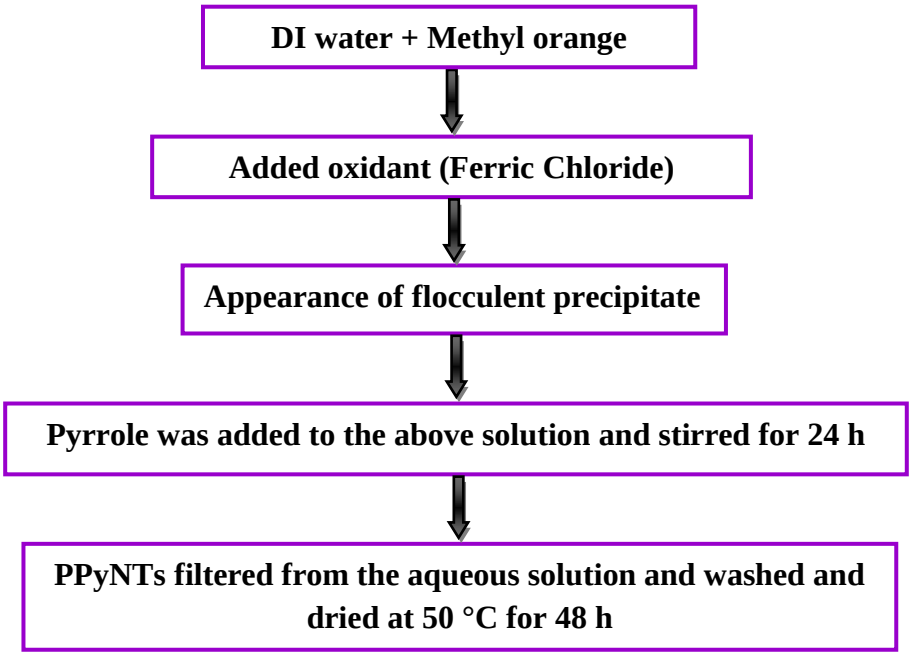

Figure 3.1: *Block diagram of synthesis of PPyNTs via reactive self-degrade MO-$FeCl_3$ template method.*

3.2.2 Synthesis of reduced graphene oxide

Reduced graphene oxide has been synthesized by the top-down method of oxidation of graphite sheets followed by chemical exfoliation and reduction of graphite oxide. Initially, graphite was oxidized to graphite oxide according to modified Hummers′ method [107] to weaken the van der Waals cohesive force and to increase the interlayer spacing between the graphite sheets. Typically, 2 g of graphite powder was added to 46 mL of concentrated H_2SO_4 and 1 g of $NaNO_3$ and the mixture was stirred for 1 h. Then, 6 g of $KMnO_4$ was added slowly in portions to the mixture in an ice bath so that the temperature did not exceed 20 °C. The resulting mixture was further stirred at 35 °C for 7 h. After 7 h of stirring, additional 6 g of $KMnO_4$ was added to the mixture in an ice bath followed by stirring for 12 h at 35 °C. A brown paste was obtained which was cooled to room temperature and diluted by adding 300 mL of water followed by the addition of 4 mL of H_2O_2. The resulting bright yellow solution was then purified by centrifugation at low speed (500-1000 rpm) by collecting the supernatant part containing graphite oxide and decanting the solid residue containing unoxidized graphite. The precipitate obtained from the supernatant part was washed repeatedly with DI water and 5% HCl till the pH became neutral. The final product was dried at room temperature to obtain graphite oxide. For the synthesis of RGO, the prepared graphite oxide was dispersed in deionized water (2 mg/mL) and ultrasonicated for 1 h to exfoliate the layers. The obtained graphene oxide suspension was then treated with reducing agent hydrazine hydrate (4 µL/mg) at 95 °C to obtain reduced graphene oxide. The obtained product was dried at 50 °C overnight. The schematic and block diagram for the synthesis process of RGO is shown in Figure 3.2 and 3.3, respectively.

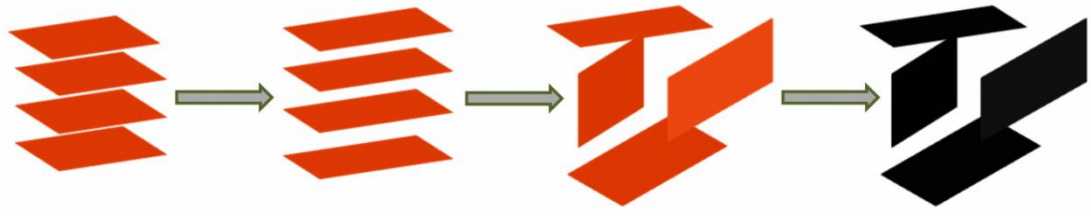

Figure 3.2: *Schematic illustration of the formation of RGO.*

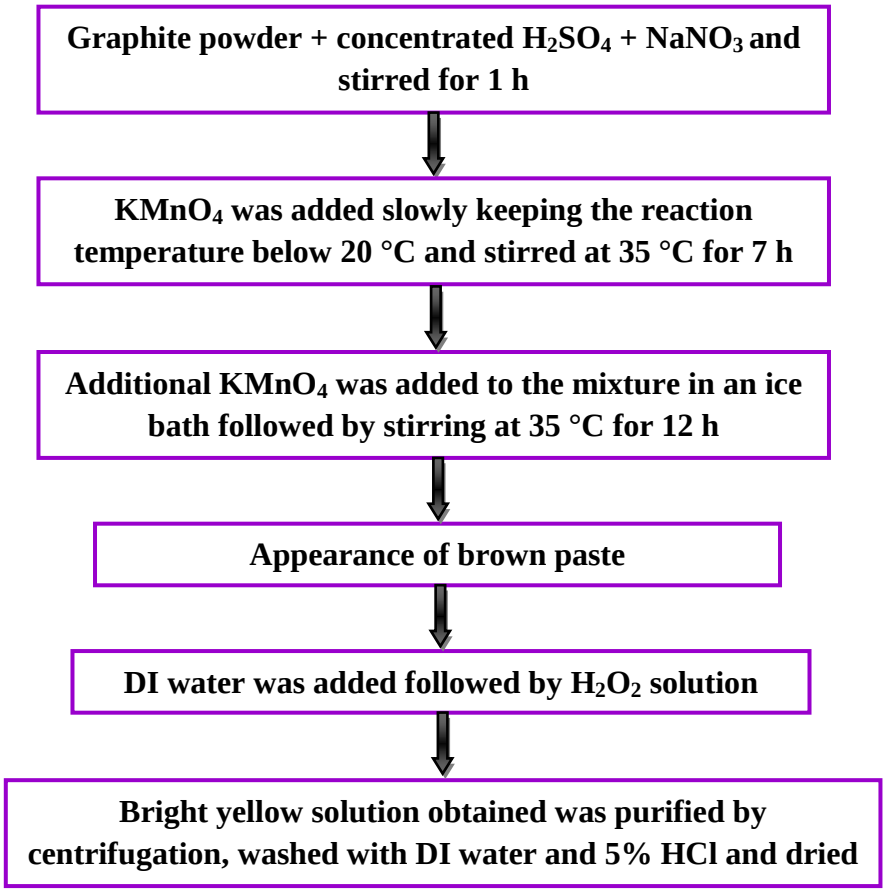

Figure 3.3: *Block diagram of synthesis of RGO via modified Hummers' method.*

3.2.3 Synthesis of reduced graphene oxide–polypyrrole nanotubes nanocomposites

RGO-PPyNTs nanocomposites have been synthesized by *in-situ* reduction of graphene oxide (GO) in presence of pre-synthesized PPyNTs to suppress the agglomeration of RGO nanosheets. For this purpose, graphite oxide was dispersed in DI water (2 mg/mL) by ultrasonication for 1 h to obtain a GO suspension. Then, 400 mg of PPyNTs was added to the GO solution and ultrasonicated for 3 h to obtain a uniform dispersion. The resulting solution was treated with hydrazine hydrate (4 mL/mg of GO) at 95 °C for 1 h to reduce the GO in the solution to RGO. The synthesized nanocomposite was washed with DI water and ethanol followed by drying at 60 °C. Four different nanocomposites were prepared by varying the concentration of GO as 5, 10, 20 and 40 wt. % with respect to PPyNTs. With increase in RGO concentration above 40 wt. %, the nanocomposite films prepared were not stable and cracked after drying due to agglomeration of RGO. The block

diagram and schematic for the synthesis of RGO-PPyNTs nanocomposites are shown in Figure 3.4 and 3.5, respectively.

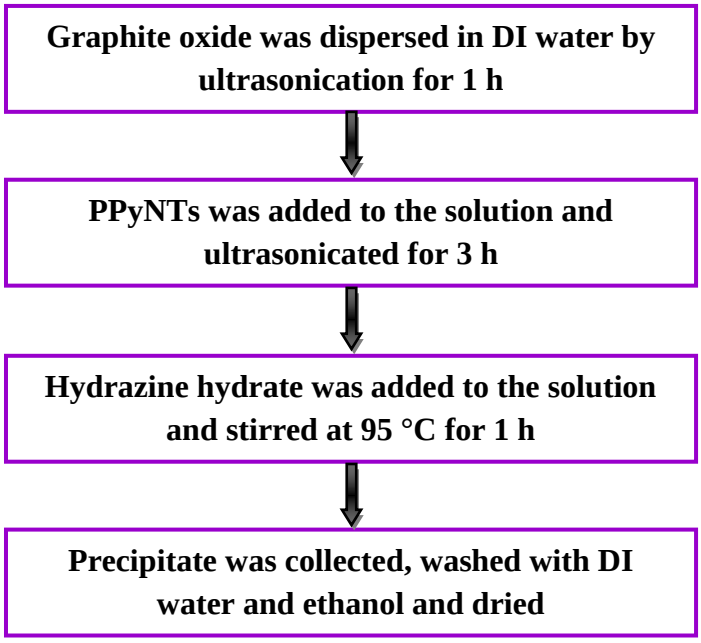

Figure 3.4: *Block diagram of synthesis of RGO-PPyNTs nanocomposites via in-situ reduction method.*

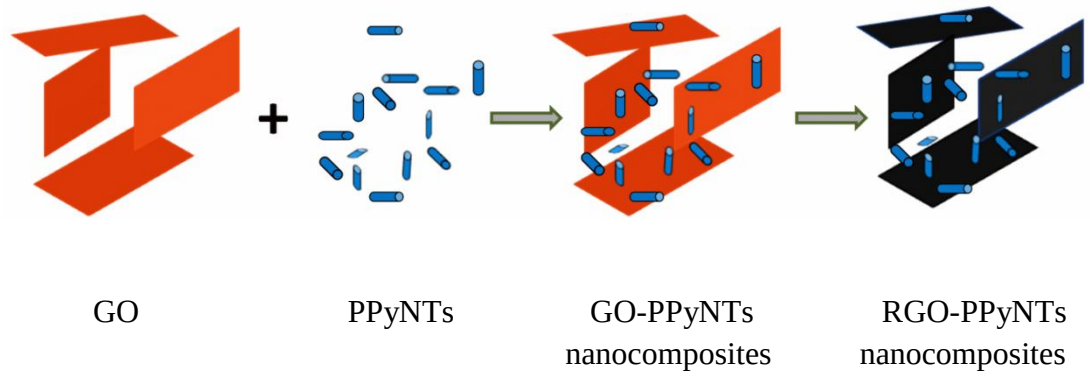

Figure 3.5: *Schematic illustration of formation of RGO-PPyNTs nanocomposites.*

3.3 Synthesis of polyaniline nanotubes and nanocomposites

3.3.1 Synthesis of polyaniline nanotubes

PAniNTs have been synthesized by reactive self-degrade template of MnO_2 nanotubes (MnO_2NTs) as reported by Chen et al. [256]. Initially, MnO_2NTs were synthesized by a hydrothermal route by dispersing 0.263 g of $KMnO_4$ in 30 mL of

DI water followed by the addition of 1 mL of concentrated HCl. The solution was then transferred into a Teflon-lined stainless steel autoclave and heated in an electric oven at 140 °C for 16 h to obtain MnO_2NTs. For the synthesis of PAniNTs, 50 mg of MnO_2NTs was dispersed in 30 mL of DI water and ultrasonicated for 1 h. Then, a solution was prepared by adding 100 µL of aniline drop-wise in 20 mL of H_2SO_4 (2.8 mL of concentrated H_2SO_4 in 17.2 mL of DI water) in an ice bath. The aniline solution was mixed rapidly with the MnO_2NTs solution and stirred vigorously in an ice bath for 6 h. MnO_2 has the ability to polymerize aniline to PAni owing to its higher potential (1.23 V) in acidic medium than that of aniline (0.5 V). Aniline gets oxidatively polymerized on the surfaces of MnO_2NTs and as the polymerization proceeds, layers of PAni get deposited on MnO_2NTs accompanied by the reduction of MnO_2 to water soluble Mn^{2+} ions. These Mn^{2+} ions can be removed from the solution by repeated washing. After 6 h of polymerization, the product obtained was washed with DI water and ethanol for several times and dried at 60 °C. The block diagram for the synthesis process is shown in Figure 3.6.

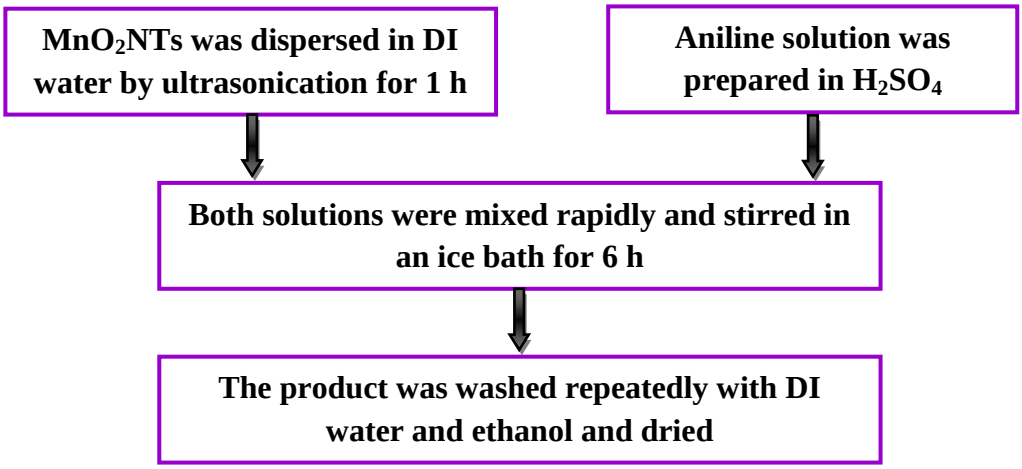

Figure 3.6: *Block diagram of synthesis of PAniNTs via reactive self-degrade MnO_2NTs template method.*

3.3.2 Synthesis of reduced graphene oxide–polyaniline nanotubes nanocomposites

Nanocomposites of RGO and PAniNTs have been synthesized by *in-situ* reduction method. Graphite oxide was dispersed in DI water (2 mg/mL) by ultrasonication for 1 h to obtain a uniform GO suspension. Subsequently, 400 mg of PAniNTs was

added to the GO solution and ultrasonicated for 3 h. The solution was then treated with hydrazine hydrate (4 µL/mg of GO) at 95 °C for 1 h to reduce the GO in the solution to RGO. During this reduction, the PAni in the nanocomposite may also have been reduced, so re-oxidation and re-protonation are required to recover the conductive PAni nanostructure. The reduced nanocomposite was then re-oxidized using ammonium peroxydisulfate by stirring overnight at room temperature. The precipitate obtained was washed with DI water and ethanol thoroughly and dried at 60 °C for 12 h. The concentration of GO was varied as 5, 10, 20, and 40 wt % with respect to PAniNTs and four nanocomposites were prepared. The highest concentration of GO was kept as 40 wt. % because the prepared nanocomposite films were not stable above this concentration due to agglomeration of RGO nanosheets. The block diagram for the synthesis process is shown in Figure 3.7.

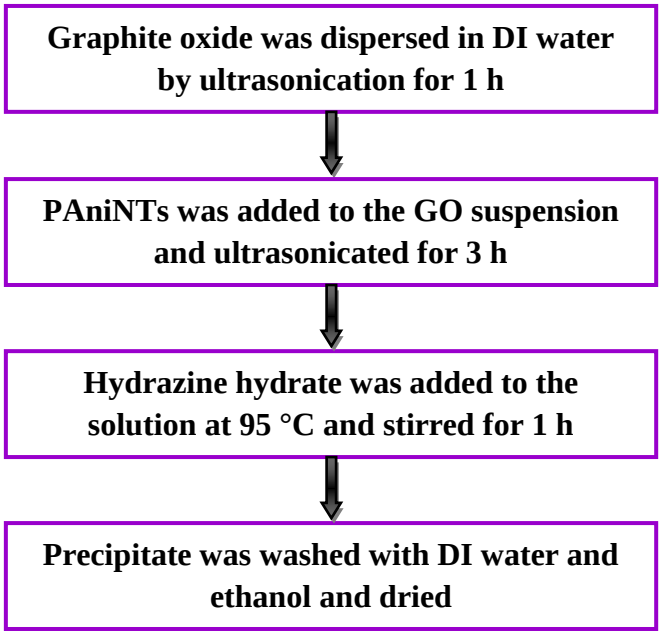

Figure 3.7: *Block diagram of synthesis of RGO-PAniNTs nanocomposite by in-situ reduction method.*

3.4 Preparation of nanocomposite electrodes

For the preparation of nanocomposite electrodes, the synthesized nanocomposite, carbon black and nafion were dispersed in a mass ratio of 85:10:5 in ethanol by ultrasonication for 30 min to form a slurry. The slurry was cast drop-wise onto 1 × 1 cm^2 ordinary glass slides for physico-chemical measurements and 1 × 1 cm^2 indium

tin oxide (ITO) coated glass slides for electrochemical measurements and dried at 50 °C. The glass slides were cleaned prior to film casting by ultrasonication stepwise in detergent solution, acetone and DI water for 15 min each followed by drying in an oven at 40 °C for several hours. The mass loading of the active material on the ITO coated glass slides was 2 mg.

3.5 Swift heavy ion (SHI) irradiation of nanocomposites

Swift heavy ion (SHI) irradiation of RGO-conducting polymer nanocomposite films has been carried out at Inter University Accelerator Centre (IUAC), New Delhi, India. The irradiation experiments were conducted in Material Science (MS) beam line under ultrahigh vacuum ~ 10^{-6} Torr. The swift heavy ions with high energies (> 1 MeV/u) are provided by the 15 UD Pelletron accelerator at IUAC.

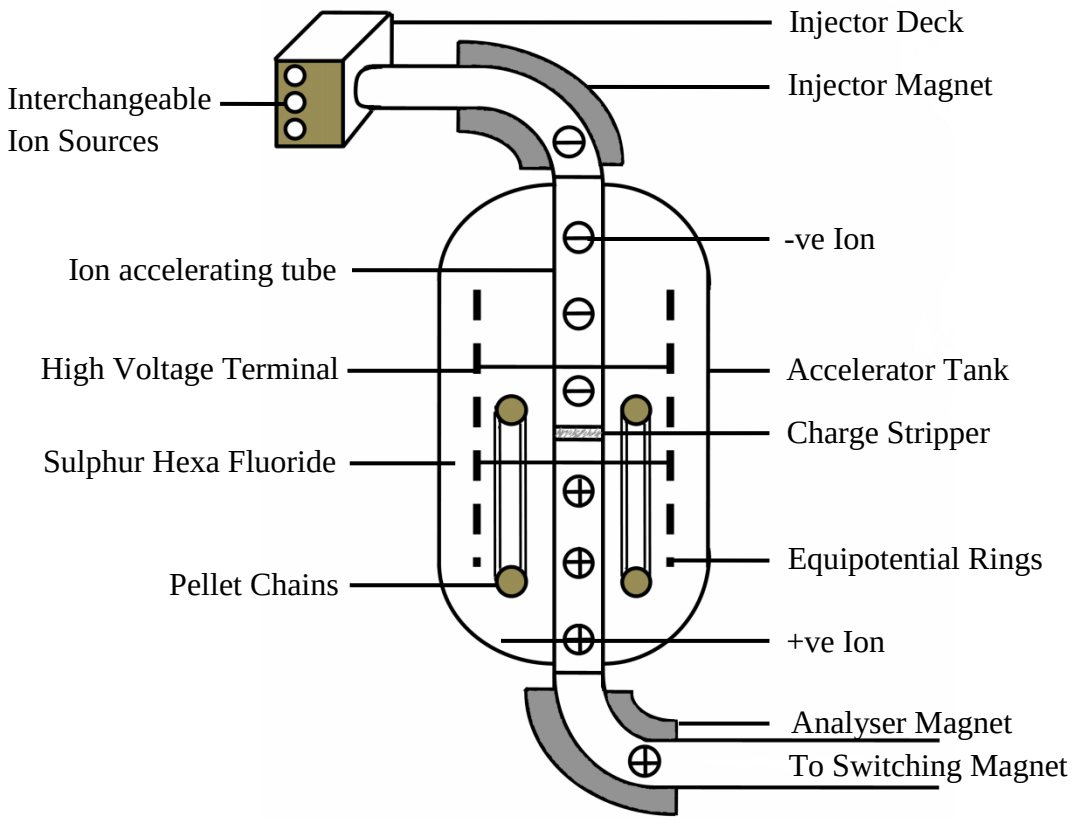

Figure 3.8: *Schematic diagram showing the principle of acceleration of ions in a Pelletron. (Courtesy: http://www.iuac.res.in/accel/pell/index.html).*

The 15 UD Pelletron accelerator at IUAC is a tandem electrostatic Van de Graff type accelerator, which exhibits a maximum terminal voltage of 16 MV and has the ability to accelerate an ion up to an energy of 200 MeV depending upon the selected ion source and the charge state. The schematic diagram of the 15 UD Pelletron at IUAC and its different parts are shown in Figure 3.8. The pelletron accelerator is comprised mainly of two parts: (a) ion source and (b) the accelerating column containing many auxiliary parts in between. The top portion of the tank consists of three different ion sources, viz., R.F. source (ALPHATROSS), Source of Negative Ions by Cesium Sputtering (SNICS) and direct extraction negative ion source (Duoplasmatron), which are capable of producing almost every type of negative ions to be injected in the pelletron tank. The working principle of these three ion sources is different. Duoplasmatron works on the principle of gas discharge, SNICS uses surface ionization and R.F. source utilizes high frequency gas discharge.

The negative ions produced by the ion source are pre-accelerated to 300 keV by the high voltage deck potential, which are then focused by several optical elements and injected into the vertical accelerating tube. The injector magnet selects the ions by their mass by bending the ions by 90° and then injects them into the accelerating tube. The singly ionized negative ions then follow a vertical downward path and are accelerated through the accelerating tube path. It consists of a vertical insulating cylindrical tank of height 26.5 m and diameter 5.5 m, filled with an insulating gas SF_6 (sulphur hexafluoride) at high pressure (> 200 psi). The top portion of the tank consists of an ion source system having a high negative potential deck, SNICS, vacuum system, power supplies and controls of the ion source required to produce and direct the negative ions into accelerating tank. The ion source system is followed by the high voltage accelerating terminal of height 3.18 m and diameter 1.52 m inside the tank. The terminal is connected to the tank vertically through ceramic titanium tubes known as accelerating tubes. A potential gradient from high voltage to ground is maintained through these tubes from top of the tank to the terminal as well as from the terminal to the bottom of the tank. An insulating column supports the high potential terminal, which consists of thirty 1 MV modules, 15 on either side of the terminal. The upper and lower portions of the column are referred to as low energy and high energy sections, respectively. A shorted section with no potential gradient, commonly known as the Dead Section, is provided each in the

low and high energy sections for equipment housing. Both are provided with an electron trap and a sputter ion pump. The low energy dead section (LEDS) also contains an electrostatic quadrupole lens while the high energy dead section (HEDS) is provided with a second foil striper assembly. It also contains a shorting rod system for temporarily shorting selected column modules without entering the pressure vessel. Two insulating shafts run, one from each ground end to the terminal and are used to drive four 400 cycles per second (cps) generators, which provide power for the equipments like heater lenses, pumps, foil changer etc., housed in the column, dead sections and terminal. The charging of high voltage terminal to 15 MV is done by using the pelletron charging chains, which have two independent sub-systems with one charging chain in each, such that each chain can supply 100 μA current. Negative ions from the ion source are focused by different optical equipments and then injected by the injector magnet into accelerator with some small energy (>> 300 keV) provided by the negative potential deck at the ion source. In the terminal, few electrons are stripped off from the negative ions by the positive ions, which are again accelerated and directed towards the bottom of the tank at the ground potential.

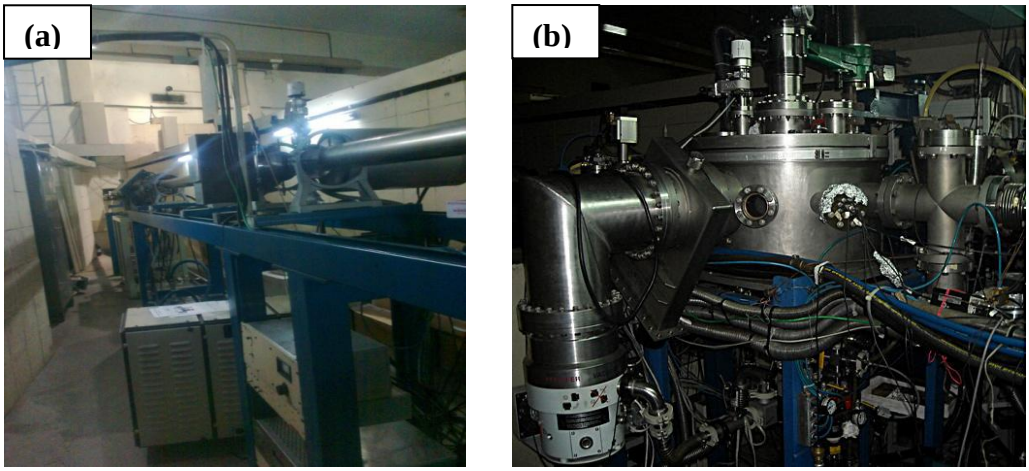

Figure 3.9: *Photographs of (a) Materials Science (MS) beam line and (b) the high vacuum irradiation chamber at IUAC, New Delhi, India.*

Figure 3.9 (a, b) shows the Materials Science (MS) beam line and the high vacuum irradiation chamber used to irradiate the samples in the present work. For SHI irradiation, the nanocomposite films were cut in 1 × 1 cm^2 area and fixed on the sample holder (ladder) made up of copper. The ladder in the MS chamber is rectangular, where 24 samples can be loaded with six samples on each side at a time.

As the sample loading is done, the ladder is inserted in the MS vacuum chamber. Vacuum inside the irradiation chamber is maintained at ~ 10^{-6} torr with the help of a rotary and turbo-molecular pump prior to irradiation. The nanocomposite systems synthesized in the present work have been irradiated at normal beam incidence.

3.5.1 Parameters related to SHI irradiation

3.5.1.1 Fluence (φ)

It is defined as the total number of irradiating ions incident per square centimeter (ions/cm^2) of the target sample. The ion fluence depends on the time of irradiation, beam current and charge state and is given by:

$$I = \frac{Q}{T} = \frac{Dqe}{T} = \frac{\varphi Aqe}{T} \tag{3.1}$$

where,

I = beam current (nA)

Q = total charge

D = dose = ion fluence (φ) in ions/cm^2 × area of irradiation (A) in cm^2

q = charge state

e = electronic charge = 1.6 × 10^{-19} C

T = time of irradiation (sec)

The time of irradiation from equation (3.1) can be written as:

$$T = \frac{\varphi A}{(I/qe)} \tag{3.2}$$

where (I/qe) is defined as the number of particles per nano ampere of beam current and is known as 1 particle nano-ampere (1 pnA = 6.25 × 10^9 particles/sec). In the present work, four different fluences of 6 × 10^{10}, 3.6 × 10^{11}, 2.2 × 10^{12} and 1.3 × 10^{13} ions cm^{-2} were chosen to irradiate the nanocomposite films. The time of irradiation was increased to increase the fluence and the required time of irradiation for a particular fluence was calculated using equation (3.2). The nanocomposite films were irradiated with the ion beam for different time intervals as per the desired fluence keeping the number of particles per nA of beam current constant at 1 pna.

3.5.1.2 Beam energy

The energy of the accelerated ion beam depends on charge state (q) of the ion and the terminal potential V_T.

$$E(MeV) = (q+1)V_T + V_{inj} \quad (3.3)$$

The 15 UD Pelletron at Inter University Accelerator Center (IUAC), New Delhi exhibits a terminal potential (V_T) in the range of 10-15 MeV and injector potential (V_{inj}) in the range of 250-350 keV. The projected range of 85 MeV C^{6+} ion beam used in the present work has been calculated using the SRIM-2007 code (SRIM-Stopping Ranges of Ions in Matter) [257]. The incident energy, corresponding electronic energy loss (S_e), nuclear energy loss (S_n) and projected range obtained from SRIM-2007 code for C^{6+} ion beam are presented in Table 3.2.

Table 3.2: *SRIM data for 85 MeV C^{6+} ions in different nanocomposite systems*

Sample	Ion	Energy (MeV)	S_e (eV/Å)	S_n (eV/Å)	Projected Range (μm)
RGO-PPyNTs nanocomposites	C^{6+}	85	23.71	0.012	222
RGO-PAniNTs nanocomposites	C^{6+}	85	27.33	0.014	163

The RGO-PPyNTs and RGO-PAniNTs nanocomposite sample showing the highest electrochemical performance studied in the present work was chosen to irradiate with 85 MeV C^{6+} ions with different fluences of 6×10^{10}, 3.6×10^{11}, 2.2×10^{12} and 1.3×10^{13} ions cm^{-2} to study the fluence dependent modifications in electrochemical properties. The energy of 85 MeV used for irradiation was evaluated in such a way that the swift heavy ions were not implanted in the nanocomposite films, but completely penetrated and passed through the films. The calculated projected range of SHI as given in Table 3.2 confirmed that the ion range was greater than the thickness of the films (~ 50-60 μm). The mass of the nanocomposite films did not change after irradiation as the ions were not implanted and passed through the films.

3.6 Characterization techniques

3.6.1 High resolution transmission electron microscopy

Figure 3.10: *High resolution transmission electron microscope (JEOL, model JEM-2100).*

High resolution transmission electron microscope (HRTEM) is a powerful tool to study the material's structure on an atomic scale. In HRTEM, a beam of accelerated electrons is passed through the specimen to create an image. An electron gun, where a tungsten filament cathode is commonly used as the electron source produces the electron beam, which is focused into a thin, coherent beam by the use of condenser lens. An anode typically at voltage of +100 keV (40 to 400 keV) with respect to the cathode accelerates the electron beam, which is focused by electrostatic and electromagnetic lenses and passed through the specimen. Parts of the electron beam are transmitted depending upon the thickness and electron transparency of the specimen. The electron beam emerging out of the specimen carries information about the structure of the specimen, which is magnified and focused by the objective lens system of the microscope onto an imaging device, such as a layer of photographic film, or a fluorescent screen, or to be detected by a sensor such as a CCD camera. The detected image is then displayed on a monitor or computer. The darker areas of the image indicate those areas of the sample where fewer electrons are transmitted through while the lighter areas of the image represent those areas where more electron transmission occurs.

The HRTEM micrographs of the samples were recorded using a high resolution transmission electron microscope (HRTEM) model JEOL JEM-2100 at SAIF, North Eastern Hill University (NEHU) as shown in Figure 3.10. The micrographs were obtained at an accelerating voltage of 200 kV at different magnifications as per requirements. For HRTEM experiments, samples were prepared by dropping a sample solution on a copper grid followed by solvent evaporation in ambient air at room temperature.

3.6.2 Scanning electron microscopy

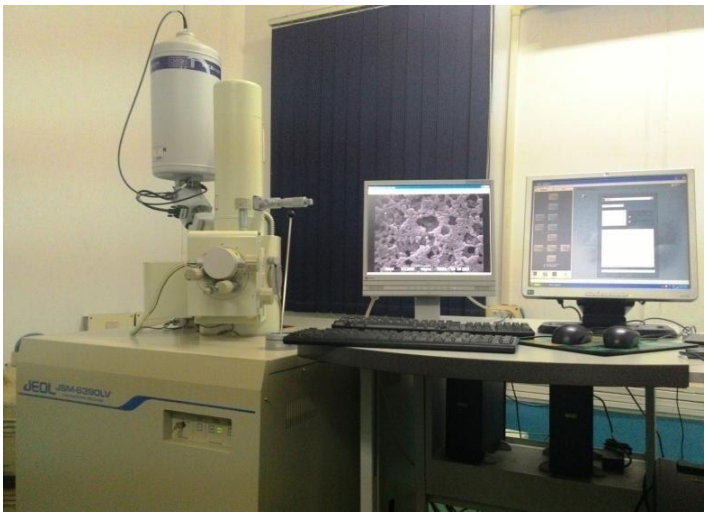

Figure 3.11: *Scanning electron microscope (JEOL, model JSM-6390 LV).*

Scanning electron microscopy (SEM) is a widely used versatile technique for materials characterization, which scans the specimen surface with a focused electron beam to create an image. An electron gun produces the electron beam having energy in the range of 0.2-40 kV by thermionic emission from a tungsten filament cathode. The accelerated electrons are then focused by condenser lenses towards the sample surface, which hits a spot of diameter around 0.4-5 nm. The position of the electron beam on the sample is controlled by scanning coils, which allow the beam to scan in a raster fashion over the sample surface. The interaction of electrons with the sample produces various types of signals that include secondary electrons, backscattered electrons, diffracted backscattered electrons and characteristic X-rays. SEM commonly detects secondary electrons and backscattered electrons for imaging samples, which provides information about the surface morphology and sample

composition. Using secondary electrons, SEM can produce images of high resolution, revealing details of less than 1 nm. Apart from imaging, SEM can be used to identify the elemental composition in the sample by measuring the wavelength of the characteristic X-rays by energy dispersive X-ray spectroscopy (EDX). SEM provides a large depth of field and varied magnification in the range of 20X to 30,000X allowing a detailed view of the sample. In field emission scanning electron microscopy (FESEM), electrons are generated by a field emission gun, which is usually a wire of tungsten shaped into a sharp point. The radius of the tungsten tip is very small (~ 100 nm), which produces a small and focused electron beam diameter. This helps FESEM to produce a cleaner image with less electrostatic distortions and improved spatial resolution < 2nm.

SEM images were obtained using a JEOL JSM 6390 LV model scanning electron microscope (shown in Figure 3.11) installed at Tezpur University, Assam, India. The micrographs were recorded at 20 kV accelerating voltage and varied magnification from 1,000 X-6,000 X. FESEM imaging was performed using a TESCAN MIRA II LMH model at Inter-University Accelerator Center (IUAC), New Delhi, India. The samples were coated with gold and placed on carbon tape before viewing.

3.6.3 X-ray diffraction

X-ray diffraction (XRD) is a commonly used non-destructive technique to obtain information about the crystal structure, phase composition, strain and crystallinity of materials. XRD peaks are produced by constructive interference of monochromatic X-rays that are scattered at specific angles from a set of lattice planes in the sample. For the generation of X-rays, a cathode ray tube produces electrons by thermionic emission that are accelerated and bombarded on the target material. When the electrons gain sufficient energy to remove electrons from the inner shell of the target material, characteristic X-rays are produced. The X-ray spectra consist of several components, the most common are the K_α and K_β radiation. The X-rays are then filtered to obtain monochromatic radiation, collimated and directed towards the sample. When the incident X-rays satisfy the Bragg's law, constructive interference occurs and a peak in intensity is observed [258]. The Bragg's law is given by:

$$n\lambda = 2d \sin\theta \tag{3.4}$$

where n is an integer, d is the interplanar spacing, θ is the diffraction angle and λ is the wavelength. A detector collects the diffracted X-rays and converts the X-ray signals into a count rate, which is displayed in a computer monitor.

The XRD patterns were recorded using a D8 Bruker AXS X-ray diffractometer (Germany) at Tezpur University, India as shown in Figure 3.12. The measurements were done using Cu K_α radiation having a wavelength of 1.5406 Å at 1°/min scan rate.

Figure 3.12: *X-ray diffraction measurement unit (D8 Bruker AXS).*

3.6.3.1 Calculation of crystallinity percentage

The crystallinity percentage of a material can be determined by XRD in terms of X-ray scattering from both the crystalline and amorphous phases in the material. The difference between scattering from crystalline and amorphous phases depends on the ordering of the material. A polymeric material can be regarded as the combination of two phase system, one crystalline and other amorphous. The inhomogeneous structure of polymers arises due to ordered chain folding (crystalline regions) separated by disordered amorphous regions. The XRD pattern of a polymeric material consists of overlapping of a broad amorphous hump with some sharp peaks as shown in Figure 3.13 (a). The total area under the diffractogram represents the sum of the amorphous hump and the crystalline peaks. Crystallinity from XRD

patterns is obtained by calculating the ratio of the areas of the crystalline peaks to the total area under the diffractogram.

If an XRD pattern consists of superposition of two crystalline peaks with areas A_1 and A_2 and a broad amorphous hump with an area A_3 as shown in Figure 3.13 (b), then the degree of crystallinity (X_C) of the polymer is given by:

$$X_C = \frac{\alpha_C(A_1 + A_2)}{\alpha_C(A_1 + A_2) + \alpha_A A_3} \tag{3.5}$$

where α_C and α_A are constants of proportionality for the crystalline and amorphous regions, respectively. For reasonable accuracy in polymers, assuming $\alpha_C = \alpha_A$ in equation (3.5) gives the degree of crystallinity as:

$$X_C = \frac{(A_1 + A_2)}{(A_1 + A_2) + A_3} \tag{3.6}$$

The degree of crystallinity can be expressed in terms of percentage by modifying the above equation (3.6) as:

$$X_C = \frac{(A_1 + A_2)}{(A_1 + A_2) + A_3} \times 100\ \% = \frac{A_c}{A_c + A_a} \times 100\ \% \tag{3.7}$$

where, $A_1 + A_2 = A_c$ represents total area of the crystalline region, $A_3 = A_a$ is the area of the amorphous region and $(A_1 + A_2) + A_3 = A_a + A_c$ represents the total area under the XRD diffractogram.

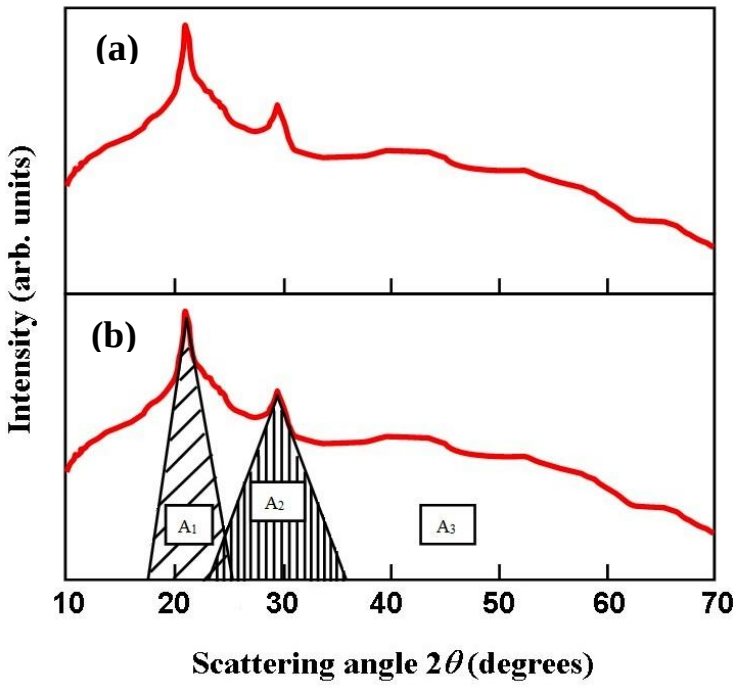

Figure 3.13: *Typical XRD pattern (a) of a semi-crystalline polymer and (b) showing the superposition of crystalline peaks and an amorphous hump.*

In the present thesis, the areas under the crystalline and amorphous regions have been measured by dividing the X-ray diffractogram into small square grids (0.5 × 0.5 mm^2) and counting the number of grids using OriginLab software. The degree of crystallinity is then calculated using equation 3.7. The degree of crystallinity of a polymer is affected by the structure of the polymer chain (ordering), the secondary valence bonds that can be formed and the molecular weight of the polymer.

3.6.4 FTIR spectroscopy

Figure 3.14: *Photograph of FTIR spectrometer (Perkin Elmer, model spectrum 100).*

Fourier transform infrared (FTIR) spectroscopy is a unique technique for the identification of functional groups and molecular structure of chemical compounds. Infrared spectroscopy involves the study of interactions between molecular vibrations and electromagnetic radiation in the infrared (IR) range. When IR radiation is passed through a material, molecules absorb some radiation and are excited to a higher vibrational or rotational energy state of the same electronic level. The molecules absorb IR radiation only if the absorption causes a change in their dipole moment. The absorbed frequency depends on the vibrational frequency of the molecules, while the absorption intensity depends on the effective change in their dipole moment. Therefore, IR spectrum provides a fingerprint of the chemical composition of a material with absorption peaks corresponding to the vibrational

frequencies of molecular bonds present in the sample. Since no two materials have the same combination of atoms, each compound has a unique IR spectrum, which allows IR spectroscopy to identify different chemical species. The intensity of the peaks in the FTIR spectrum directly implies the presence of the chemical bond.

FTIR spectroscopy of the samples was performed using a Perkin Elmer Spectrum 100 (Figure 3.14) spectrophotometer installed at Tezpur University, Assam, India. The samples were pressed with standard potassium bromide (KBr) in pellet form and the spectra were recorded in the range of 400-4000 cm^{-1} with a resolution of 1 cm^{-1}.

3.6.5 Micro-Raman spectroscopy

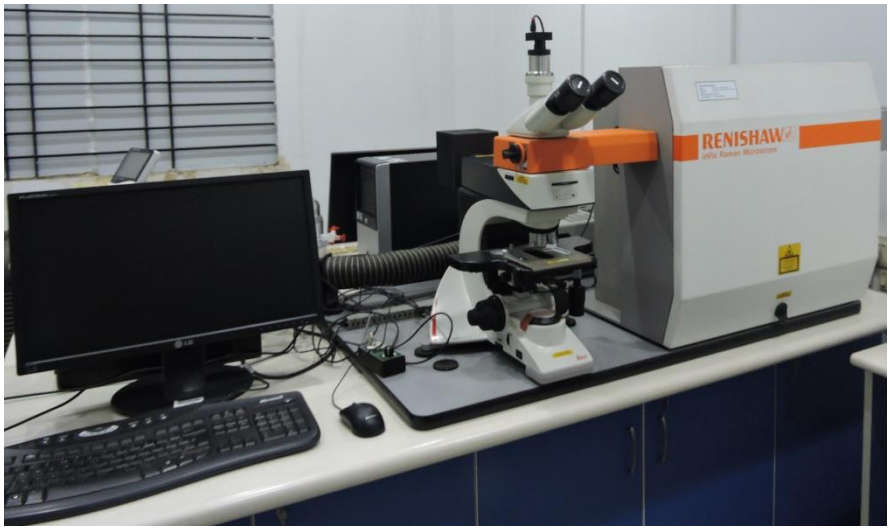

Figure 3.15: *Photograph of micro-Raman spectrometer (Renishaw inVia).*

Raman spectroscopy is one of the most powerful laser spectroscopic method for identification molecular vibrations and structural defects of a material. It differs from IR spectroscopy from the fact that a molecule exhibit Raman effect if there occurs a change in its polarizability. Raman spectroscopy is a study of the interaction between monochromatic light and matter, in which the light is inelastically scattered [259]. During the inelastic process, energy is transferred between the incident photons and the molecules such that the energy of the scattered photon is higher or lower than that of the incident photon. The Raman scattering is a very weak process and only one photon out of 10^6-10^8 scattered photons is Raman scattered. The inelastically scattered light is collected with a lens and is sent through a spectrophotometer to

obtain the Raman spectrum of the material, which is a plot of the intensity of scattered light as a function of shift in wavenumber from the original laser line. The peak positions determine the vibrational energies of molecular bonds of the sample.

The micro-Raman spectra were recorded using a Renishaw inVia spectrometer (Renishaw, Wotton-under-Edge, UK) as shown in Figure 3.15 in the range of 500-3000 cm^{-1} at a resolution of 0.3 cm^{-1}. An argon ion laser with a wavelength of 514.5 nm was used as the excitation source.

3.6.6 Thermogravimetric analysis

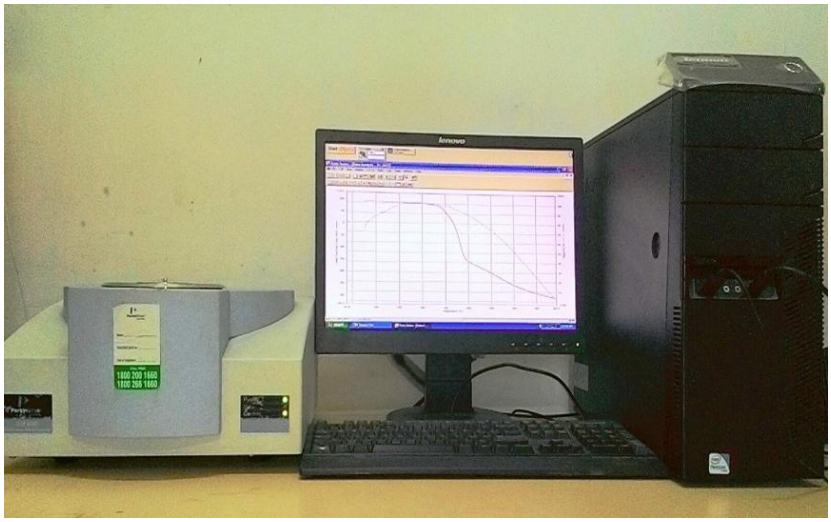

Figure 3.16: *Photograph of thermogravimetric analyzer (Perkin Elmer, model STA 6000).*

Thermogravimetric (TG) analysis is a thermal analysis method in which mass changes of a substance are measured as a function of temperature with constant heating rate or with constant temperature (isothermally) as a function of time. The measurement provides information about various physico-chemical phenomena of a substance such as phase transitions, absorption and desorption, vaporization, thermal decomposition etc. A thermogravimetric analyzer consists of a sample pan with a precision electronic microbalance located inside the furnace. A programmed temperature control increases the temperature of the sample pan at a constant rate during the experiment. The atmosphere of the sample chamber is filled with an inert gas to avoid oxidation or other undesired reactions. Various components of the samples are decomposed with increase in temperature and the percentage of weight

loss is recorded as a function of temperature. The themogravimetric data is collected and graphed as weight percent along Y-axis and temperature along X-axis. TG analysis is primarily used to determine the thermal stability of a substance up to temperatures of 1000 °C. The first derivative of TG curves may be plotted with respect to temperature for in-depth interpretations of thermal decomposition rate and temperature.

The thermal stabilities of the samples were analyzed using a Perkin Elmer, model STA 6000 thermal analyzer (Figure 3.16) with a dynamic nitrogen flow of 20 ml min^{-1} and a heating rate of 20 °C min^{-1}. The thermal decomposition of the samples was monitored in the temperature range of 50-800 °C.

3.6.7 Current-voltage characteristics

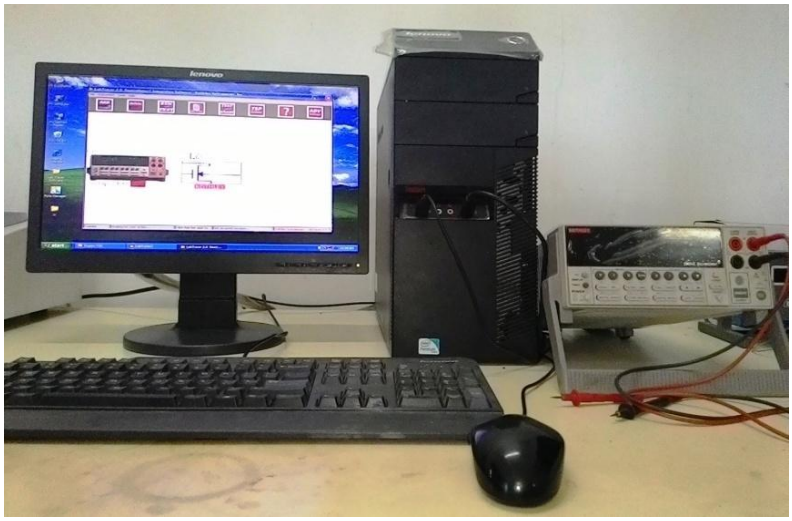

Figure 3.17: *Photograph of two-probe current-voltage measurement system (Keithley, model 2400-C).*

The electrical conductivity of materials can be measured using two methods: two-probe and four-probe current-voltage (I-V) measurements. The two-probe method is simpler and commonly used for studying the I-V characteristics of samples. Current-voltage characteristic is a curve representing the variation of electric current with respect to the applied voltage. In two-probe method, two contacts are made on the sample surface by thin lead wires and the current flow across the two ends of the sample is measured by varying the voltage. Four-probe measurement set-up consists of four probes equally spaced about 1 mm apart in a straight line. The probes are

mounted in a teflon bush, which ensures good electrical insulation between them. The probe arrangement is mounted in a suitable stand which holds the sample plate. Current is applied between the outer two probes and voltage is measured across the inner two probes. For a known value of current and by measuring the voltage, the resistivity of the samples of known thickness can be calculated. The reciprocal of resistivity gives the conductivity of the samples. Four-probe method is the more commonly accepted technique for electrical conductivity measurement.

The current-voltage characteristics of the samples were studied by two-probe measurements in the applied voltage range of -5 V to 5 V using Keithley source meter model 2400-C interfaced with a PC as shown in the Figure 3.17. The dc conductivities of the samples were measured using SES Instruments, Roorkee, India model DFP-02 four-probe measurement set-up (Figure 3.18) at room temperature. In case of RGO-PPyNTs and RGO-PAniNTs nanocomposites, the samples were prepared in pellet form of 5 mm diameter and 1 mm thickness for the measurements, while for irradiated RGO-PPyNTs and RGO-PAniNTs nanocomposites, the measurements were conducted in film form.

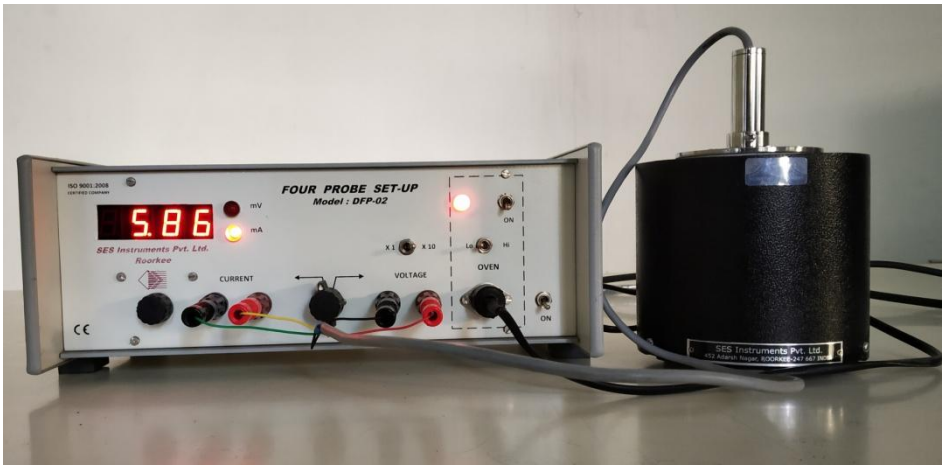

Figure 3.18: *Photograph of four-probe conductivity measurement set-up (SES Instruments, Roorkee, India, model DFP-02).*

3.6.8 N_2 adsorption-desorption measurements

Gas adsorption manometry method is used for the measurement of adsorption and desorption isotherms of nitrogen at liquid N_2 temperature of 77 K. The sample chamber is evacuated at 120-200 °C followed by cooling to liquid N_2 temperature of

77 K. Consecutive known amounts of N_2 adsorbate is introduced into the sample chamber and the pressure of nitrogen is gradually increased. The sample will adsorb some quantity of gas, which causes the pressure to decrease slowly until an equilibrium pressure is established. After stabilization, the equilibrated pressure is noted and the amount of nitrogen adsorbed at each equilibrated pressure is recorded. The pressure of nitrogen over the sample is gradually increased until it reaches near saturation pressure, where the adsorption process is complete. The desorption isotherm is then obtained by reducing the pressure step-wise until the starting value of pressure over the sample is reached. The adsorption-desorption isotherms are obtained by plotting the volume adsorbed along Y-axis and relative pressure along X-axis.

Nitrogen adsorption-desorption isotherms of the samples were measured using a Quantachrome (NOVA 1000E) analyzer (Figure 3.19) at liquid N_2 temperature of 77 K. The specific surface areas of the samples were determined using Brunauer-Emmett-Teller (BET) method from the adsorption data. The pore size distribution curves were obtained from the desorption data using the Barrett-Joyner-Halenda (BJH) method

Figure 3.19: *Set-up used for measurement of N_2 adsorption-desorption isotherms (Quantachrome, model NOVA 1000E).*

3.6.9 Contact angle measurements

The wettability of a solid surface by a liquid is quantified by contact angle measurements. Contact angle is defined as the angle formed between a liquid drop and solid surface at the interface where the solid and liquid intersect [260]. The contact angle values of solid samples are measured using contact angle meter or optical tensiometer. The sample surface is held in horizontal position and 8-10 µL of the testing liquid is dropped gently onto the surface by a syringe needle. The drop image is captured with a high resolution camera when the liquid drop is resting on the surface and not moving. The drop shape is then fit with a tangent line drawn from the baseline of the drop to the edge to determine the contact angle value. Contact angle is directly related to the interfacial tension between the liquid and the solid and therefore the measurement of contact angle on a given surface with two or more liquids can be used to determine the surface free energy of the solid [245].

Contact angle measurements of the samples were carried out at room temperature using Data physics instrument GmbH contact angle measurement system, model OCA 15 EC, Germany (Figure 3.20). To determine the surface free energy of the samples, contact angles were measured using two different liquids, one polar: water and other non-polar: diiodomethane. The Owens, Wendt, Rabel and Kaelble (OWRK) method was used for the calculation of surface free energy.

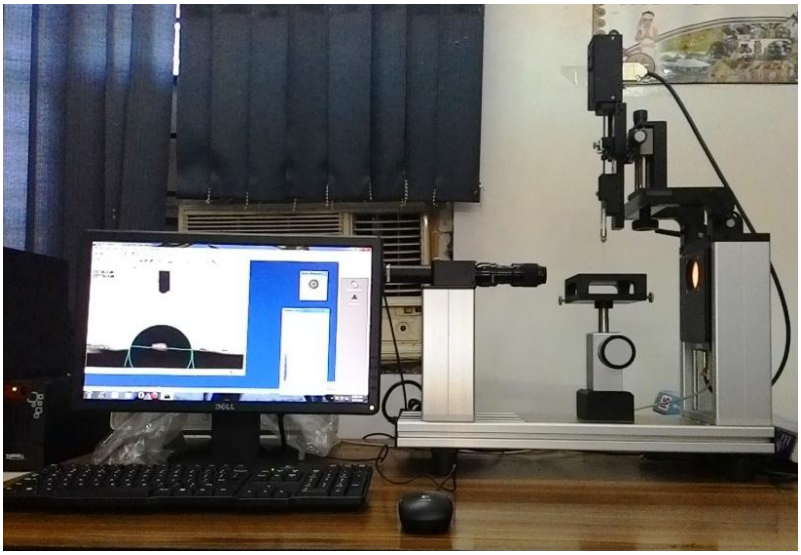

Figure 3.20: *Set-up used for measurement of contact angle (Data Physics, model OCA 15 EC).*

3.6.10 Measurements of electrochemical properties

The electrochemical measurements were performed using an Autolab PGSTAT302N potentiostat/galvanostat (Metrohm Autolab, Netherlands) in a three-electrode system as shown in Figure 3.21. The nanocomposite films prepared on ITO coated glass slides were used as the working electrode and a platinum wire was used as the counter electrode. The measurements were carried out in 1 M KCl electrolyte for RGO-PPyNTs system and 1 M H_2SO_4 electrolyte for RGO-PAniNTs system. All the potentials were measured with reference to Ag/AgCl reference electrode (3M KCl, 0.210 V vs. standard hydrogen electrode (SHE)).

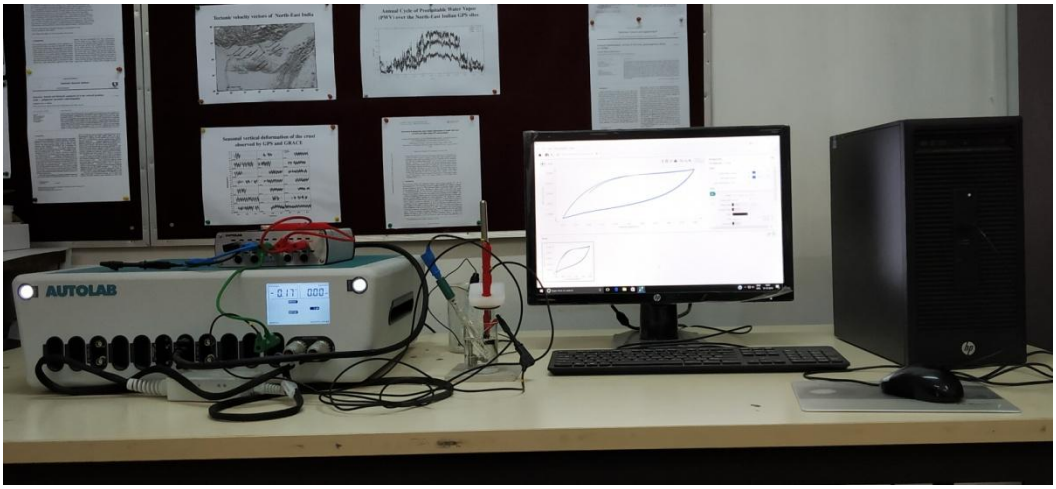

Figure 3.21: *Photograph of Autolab PGSTAT302N potentiostat/galvanostat (Metrohm Autolab, Netherlands).*

(i) Cyclic voltammetry

Cyclic voltammetry (CV) provides information about the charge transfer kinetics and redox processes of electrode materials. CV was performed by scanning the potential of the working electrode at different sweep rates and measuring the output current. The cyclic voltammograms of the electrode materials were recorded in a potential range of 0.2–0.8 V at different voltage scan rates of 10, 25, 50, 75 and 100 mV s^{-1} with a step potential of 2.44 mV.

(ii) Galvanostatic charge-discharge measurements

Galvanostatic charge-discharge (GCD) measurements were conducted to study the charge-discharge behavior and to determine the specific capacitance of the synthesized electrodes. It is a chronopotentiometry method where the electrode is charged and discharged within a fixed voltage range at constant current densities. GCD measurements were carried out in the voltage range of 0-0.8 V at various constant current densities of 0.5, 1 and 1.5 A/g in a three-electrode configuration.

(iii) Electrochemical impedance spectroscopy

Electrochemical impedance spectroscopy (EIS) was performed to measure the equivalent series resistance, charge transfer resistance and Warburg impedance of the electrode materials. The EIS measurements were carried out using Autolab PGSTAT302N potentiostat/galvanostat (Metrohm Autolab, Netherlands) in the frequency range of 10 mHz to 50 kHz at an AC voltage amplitude of 10 mV at room temperature. The measurements were conducted in a three-electrode arrangement using a platinum counter electrode and Ag/AgCl reference electrode (3M KCl). The films prepared on ITO coated glass slides were used as the working electrodes.

(iv) Cyclic stability study

Cyclic stability determines the cycle life of an electrode i.e. the number of charge-discharge cycles sustained by an electrode during its lifetime. The cycle life was determined by calculating the capacitive retention (capacitance recovery) of the synthesized electrodes for 1000 cycles. Cyclic voltammograms of the electrodes were recorded at a scan rate of 10 mV s^{-1} for 1000 cycles. The capacitive retention is calculated from the specific capacitance values of the 1^{st} and 1000^{th} cycle.